

MAGNIFICENT MAGNIFICATION: EXPLOITING THE OTHER HALF OF THE LENSING SIGNAL

ERIC M. HUFF^{1,2} & GENEVIEVE J. GRAVES^{1,2,3}*Draft version September 6, 2018*

ABSTRACT

We describe a new method for measuring galaxy magnification due to weak gravitational lensing. Our method makes use of a tight scaling relation between galaxy properties that are modified by gravitational lensing, such as apparent size, and other properties that are not, such as surface brightness. In particular, we use a version of the well-known fundamental plane relation for early type galaxies. This modified “photometric fundamental plane” replaces velocity dispersions with photometric galaxy properties, thus obviating the need for spectroscopic data. We present the first detection of magnification using this method by applying it to photometric catalogs from the Sloan Digital Sky Survey. This analysis shows that the derived magnification signal is comparable to that available from conventional methods using gravitational shear. We suppress the dominant sources of systematic error and discuss modest improvements that may allow this method to equal or even surpass the signal-to-noise achievable with shear. Moreover, some of the dominant sources of systematic error are substantially different from those of shear-based techniques. Thus, combining the two techniques addresses the major weaknesses of each and provides a substantial improvement over either method used in isolation. With this new technique, magnification becomes a necessary measurement tool for the coming era of large ground-based surveys intending to measure gravitational lensing.

Subject headings: cosmology: observations — gravitational lensing: weak — methods: observational

1. INTRODUCTION

The modern cosmological concordance model has been spectacularly successful. This success has come at a price, however: cosmologists must postulate a universe in which the vast majority of the content, in the form of dark matter and dark energy, is inaccessible to direct observation.

Gravitational lensing, and weak lensing in particular, provide our best window onto the dark universe. Because of this, the astronomical community is investing heavily in current and future imaging surveys, both ground- and space-based, designed at least in part around weak lensing science, e.g., the Dark Energy Survey (DES), the Panoramic Survey Telescope and Rapid Response System (Pan-STARRS), the Hyper Suprime Cam for the *Subaru* telescope, the Large Synoptic Survey Telescope (LSST), and Euclid.

Lensing measurements have already played a significant role in astrophysics in the last two decades over a range of scales and physical regimes. Weak lensing measurements have characterized the aggregate properties of galaxies’ dark matter haloes, (e.g., Fischer et al. 2000; Sheldon et al. 2004; Hoekstra et al. 2004; Seljak et al. 2005; Mandelbaum et al. 2006b; Parker et al. 2007), the dark matter profiles of large galaxy clusters, both on a cluster-by-cluster basis (e.g., Kneib et al. 2003; Broadhurst et al. 2005; Clowe et al. 2006; Hoekstra 2007; Jee et al. 2007; Mahdavi et al. 2007a,b; Bergé et al. 2008; Bradač et al. 2008; Okabe & Umetsu 2008; Kubo et al. 2009) and for stacked galaxy groups and clusters (e.g., Mandelbaum et al. 2006a; Sheldon et al.

2009; Leauthaud et al. 2010) and, with recent cosmic shear detections (Fu et al. 2008; Massey et al. 2007), directly measured the clustering of matter on cosmological scales.

These measurements are currently made almost exclusively by studying spatially-correlated distortions in the ellipticities of background galaxies due to the shear component of the gravitational lensing distortion. In the weak-lensing regime, the ellipticities induced by lensing are small ($\sim 1\%$) compared to the range of intrinsic galaxy ellipticities ($\sim 30\%$) (Mandelbaum et al. 2005).

The lensing distortion also magnifies background sources, but the intrinsic variance in the distribution of galaxy sizes and luminosities—those properties perturbed by magnification—is much larger than that of galaxy shapes. Magnification measurements to date have necessarily had to average over much larger galaxy samples to obtain signal-to-noise (S/N) equivalent to shear measurements (Hildebrandt et al. 2011; Bauer et al. 2011; Ménard et al. 2010; Scranton et al. 2005).

In this Letter, we make use of a tight galaxy scaling relation—a photometry-only version of the well-known fundamental plane for early type galaxies (Djorgovski & Davis 1987; Dressler et al. 1987)—to substantially narrow the intrinsic distribution of sizes for a set of background source galaxies. This makes it possible to measure the weak lensing magnification signal around a set of foreground galaxy lenses with higher S/N than was previously thought possible (Rozo & Schmidt 2010). A thorough description of the methodology and implementation of this analysis will be presented in a forthcoming paper (hereafter Paper II). Here, we describe the core concepts, present a detailed outline of the method, and demonstrate its effectiveness.

In section 2, we describe the scaling relation used in

¹ Department of Astronomy, University of California, Berkeley, CA 94720, USA

² Lawrence Berkeley National Lab, 1 Cyclotron Road MS50R, Berkeley, CA 94720

³ Miller Fellow

this analysis. In section 3, we present a proof-of-concept measurement of weak lensing magnification using this technique and control for the most important systematic biases. We conclude in section 4 with a brief discussion of the ways this method might be improved upon, with an eye toward extracting a lensing signal from magnification that equals or even exceeds the S/N obtainable from shear-based techniques. Throughout, we assume a Λ CDM cosmology with $\Omega_M = 0.274$, $\Omega_\Lambda = 0.726$, and $H_0 = 100 \text{ km s}^{-1} \text{ Mpc}^{-1}$.

2. THE PHOTOMETRIC FUNDAMENTAL PLANE

The fundamental plane (FP) is in many ways an ideal tool for measuring magnification. It is an observed correlation between galaxy effective radius (R_e), which is magnified by gravitational lensing, and two galaxy properties which are unaltered by lensing: galaxy surface brightness (μ) and the stellar velocity dispersion (σ). The intrinsic scatter in the FP is ~ 0.08 dex (Jørgensen et al. 1996; Bernardi et al. 2003), or 20%. Thus the FP makes it possible to predict the intrinsic value of R_e from observations of μ and σ , which can then be compared with the observed values of R_e to measure magnification.

The FP was in fact proposed as a tool for this purpose by Bertin & Lombardi (2006), but to our knowledge has never been used as such due to a critical flaw. Placing galaxies on the FP requires σ measurements. Even with the tight scatter in the FP, a statistically viable measurement would require high-resolution spectroscopic measurements for millions of galaxies.

Identifying a purely photometric analog to the FP with comparable scatter would solve this problem. Such a relation has already been identified by Graham (2002), where the concentration of the galaxy light profile fills the role normally served by σ . This works in part because concentration and velocity dispersion are both strongly correlated with galaxy mass, and in part because at fixed mass, galaxies with more concentrated mass profiles have higher velocity dispersions. We will explore the relation between the spectroscopic fundamental plane and the photometric relation deployed here more fully in Paper II.

2.1. Background Sources

To define a photoFP for this work, we use a sample of galaxies drawn from the Sloan Digital Sky Survey III (SDSS-III) Eighth Data Release (DR8, Aihara et al. 2011). We limit the sample to resolved sources that meet basic quality cuts (e.g., are not saturated). For these, we estimate photometric redshifts (photo- z 's) based on the SDSS *ugriz* photometry using the public code ZEBRA (Feldmann et al. 2006) run with the default templates, allowing interpolation between the standard templates without template optimization. To select a sample of early type background sources that should lie on the photoFP, we exclude the $\sim 2/3$ of the galaxies with best-fitting templates inconsistent with that of a passive stellar population. The sample selection for background sources will be described in greater detail in Paper II.

The SDSS photometric pipeline does not measure Sérsic index. Here, we substitute for n the SDSS petrosian concentration $C = R_{90}/R_{50}$, defined as the ratio of the radii containing 90% and 50% of the Petrosian flux

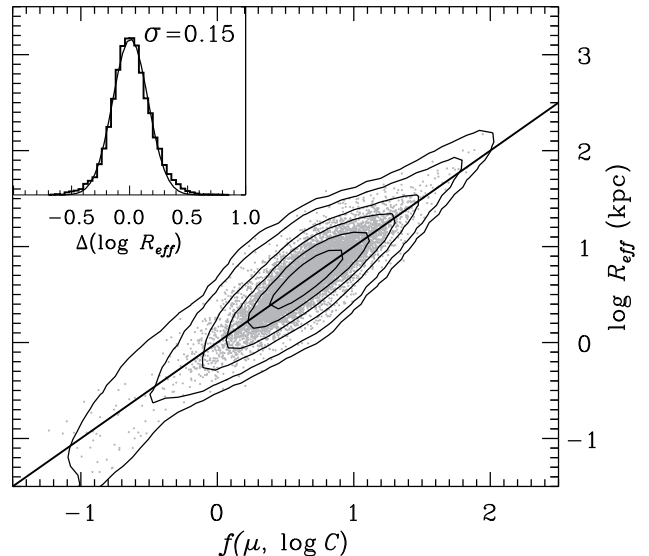


Figure 1. The photometric fundamental plane for our source sample of 8.4 million galaxies, shown edge-on. $\log R_e$ is fit as a function of effective surface brightness (μ) and concentration ($\log C$) separately in redshift bins of width $\Delta z = 0.01$. Gray points show a random subset of 100,000 galaxies from the source catalog, while the solid line shows the one-to-one relation. Contours enclose the 0.5σ , 1σ , 1.5σ , 2σ , 2.5σ , and 3σ boundaries of the 2D distribution for the full source catalog. The inset shows the distribution of residuals in $\log R_e$ from the photoFP fits, which has width $\sigma = 0.153$ dex.

(e.g., Shimasaku et al. 2001). All reported quantities are measured in the r band.

We fit a photoFP of the form

$$\log R_e = \alpha\mu + \beta \log C + \gamma, \quad (1)$$

where R_e is the half-light radius of the best-fit de Vaucouleurs light profile converted into physical units using the ZEBRA photo- z , μ is the mean de Vaucouleurs surface brightness within R_e , and α , β , and γ are free parameters. To avoid errors resulting from a redshift-dependent selection function, evolution in the photoFP, and K -corrections to the radii due to the fact that the morphological measurements are all made in the observed-frame r band, we divide our galaxy sample into redshift bins with width $\Delta z = 0.01$ and fit the photoFP separately in each bin. The best-fit coefficients are chosen to minimize the dispersion in effective radius at fixed μ and $\log C$, taking into account only the errors in R_e .

Figure 1 shows an edge-on view of the photoFP for our source sample. The dispersion around the photoFP in the direction of effective radius is 0.15 dex, or 35%.

2.2. Magnification using the photoFP

A line-of-sight matter overdensity at lens redshift z_l will produce an image convergence κ of amplitude:

$$\kappa = \frac{\Sigma(d_l \vec{\theta})}{\Sigma_{\text{crit}}}, \quad (2)$$

where Σ is the projected surface density on the sky at z_l and Σ_{crit} is the characteristic surface density of matter required for lensing. Σ_{crit} is defined by the lensing geometry, such that

$$\Sigma_{\text{crit}} = \frac{c^2}{4\pi G} \frac{d_s}{d_l d_{ls} (1 + z_l)^2}, \quad (3)$$

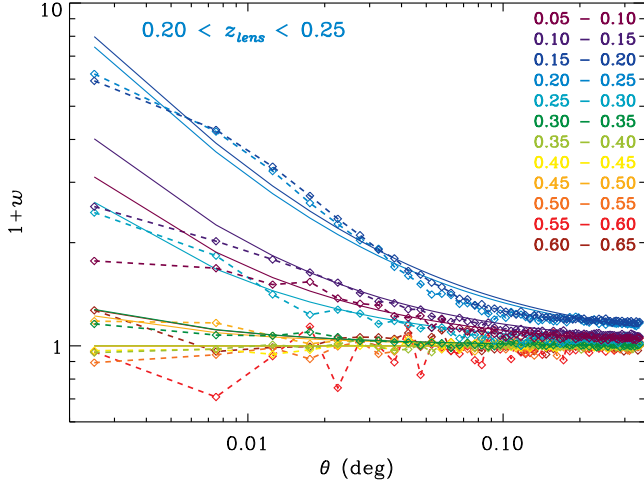


Figure 2. The projected correlation function for sources around lenses with $0.20 < z_l < 0.25$. Colors indicate different bins in z_s . Solid lines show fits to the data. At small separations, a large fraction of the galaxies in nearby z bins are likely scattered in from z_l through photo- z errors. See text for details.

where d_l , d_s , and d_{ls} are the angular diameter distances from the observer to the lens, from the observer to the source, and from the lens to the source, respectively. The factor of $(1 + z_l)^2$ arises from our use of comoving coordinates.

The lensing convergence re-scales the light profile, in the limit of very weak lensing, by a factor of $(1 + \kappa)$. The radius and luminosity increase, but as the light profile is simply rescaled, the concentration is left unchanged. In the presence of the scaling relation described above, this implies an estimator $\hat{\kappa}$ of:

$$\begin{aligned} \log(1 + \hat{\kappa}) &= \Delta \log R_e \\ &\equiv \log R_e - (\alpha\mu + \beta \log C + \gamma). \end{aligned} \quad (4)$$

If the errors in the observables are uncorrelated, the variance in our estimator $\hat{\kappa}$ is just the variance in the photoFP in the direction of R_e . We extract a galaxy-galaxy lensing signal by cross-correlating this estimator with a population of foreground lenses.

3. A MAGNIFICATION MEASUREMENT

3.1. Lens Sample

The lens sample is selected from the NYU Value-Added Catalog (Blanton et al. 2005) version of the SDSS Data Release 7 (DR7) spectroscopic survey (Abazajian et al. 2009), using only Luminous Red Galaxy Sample targets (LRGs, Eisenstein et al. 2003). In order to compare with the results of Mandelbaum et al. (2008a), we limit the sample to massive galaxies with absolute r -band magnitudes $-21.5 > M_{0.0r} > -22.6$ and redshifts $0.15 < z < 0.35$. The magnitudes are k -corrected and evolution corrected to $z = 0.0$ as in Mandelbaum et al. (2006a, hereafter M+06). Finally, to exclude satellite galaxies that are not at the centers of their dark matter haloes, we remove galaxies with brighter nearby LRGs, again following M+06. This gives a sample of $\sim 55,000$ lenses that have comparable properties to the combined LRG sample of M+06.

3.2. Correcting Biases due to Photometric Redshift Errors

In the presence of photo- z errors, the overdensity of sources clustered near a lens will produce an excess of galaxies with incorrect photo- z (z_p) along the line of sight to the lens. As a result, when we average $\Delta \log R_e$ over the foreground or background source galaxies, we systematically mis-estimate the residuals from the plane associated with a lens due to the ‘shadow’ cast by photo- z errors.

To deal with this bias, we will calculate the magnitude of this spurious signal directly from the data, and subtract it from our measured signal. We must first estimate the error in $\Delta \log R_e$ induced by a galaxy being assigned the wrong z_p ($\Delta \log R_e^{\text{err}}$), then calculate what fraction f_l of the galaxies at each z_p have been scattered in from z_l . In these terms, the observed mean photoFP residual is:

$$\Delta \log R_e^{\text{obs}} = (1 - f_l) \log(1 + \kappa) + f_l \Delta \log R_e^{\text{err}}, \quad (5)$$

where κ is the true convergence.

$\Delta \log R_e^{\text{err}}$ can be estimated by assuming that the galaxy lies on the photoFP at z_l but is incorrectly assigned to z_p . The inferred effective radius of a galaxy with true redshift z_l that is mistakenly assigned to z_p will be off by a factor of $d_s(z_p)/d_s(z_l)$. The surface brightness dimming correction will be similarly incorrect, with $\mu_p = \mu_l - 10 \log[(1 + z_p)/(1 + z_l)]$. Finally, the photoFP fits differ between redshift bins. A galaxy with an incorrect photo- z will therefore lie off the photoFP in its assigned redshift bin by

$$\Delta \log R_e^{\text{err}} = \log \left(\frac{d_s(z_p)}{d_s(z_l)} \frac{R_e^p(\mu_p, C)}{R_e^l(\mu_l, C)} \right). \quad (6)$$

The expressions $R_e^p(\mu_p, C)$ and $R_e^l(\mu_l, C)$ are the radii that would be predicted by the photoFP for that galaxy’s surface brightness and concentration in the bins corresponding to z_p and z_l , respectively.

The quantity f_l can be estimated by cross-correlating the positions of sources at z_p with lenses at z_l . We assume that the positions of galaxies in widely separated redshift bins are uncorrelated and that any observed excess of sources far behind a lens is due to scattering from z_l . This means that

$$f_l = \frac{w_{il}(\theta)}{1 + w_{il}(\theta)}, \quad (7)$$

where $w_{il}(\theta)$ is the angular cross-correlation between the positions of sources at z_i and lenses at z_l . A cross-correlation signal of this form can also be produced by the boosted number counts of magnified background sources (e.g., Jain & Lima 2011) but that effect is too weak to detect with a lens sample of this size.

The cross-correlations for $0.20 < z_l < 0.25$ with a range of z_s bins are shown in figure 2. We fit an angular correlation function of the form

$$1 + w_{il}(\theta) = \frac{A_{il}}{\theta^{0.8}} + B_{il} \quad (8)$$

where A_{il} and B_{il} are free parameters. The choice of power law index is motivated by the angular correlation function measurements of Wake et al. (2011), which are

in agreement with our observed w_l . Incorrectly estimating the true mean density of galaxies at z_p will cause B_{il} to deviate from unity, as is observed. We remove the effects of this uncertainty when calculating f_l by setting $B_{il} = 1$. Sources with $f_l > 0.20$ (above the black horizontal line in Figure 2) are excluded from the lensing measurement, while sources with $f_l < 0.20$ are corrected using equation 5.

In addition to the effects of galaxy clustering on photometric redshift errors, a mean offset between the true and photometric redshifts in a z_p bin will cause an incorrect estimation of the critical density Σ_{crit} for all of the galaxies in that bin. This error depends on the distribution of foreground lens redshifts. Using the method of Mandelbaum et al. (2008b), we estimate the effect of a mean shift in our photo- z 's on the signal of no more than 10%. This uncertainty is small relative to the other corrections discussed here, so we defer this calculation to Paper II.

3.3. Sky Proximity Bias Correction

The SDSS photometric pipeline produces known sky subtraction proximity effects, where the photometry of objects near bright stars or galaxies is systematically biased (c.f. Aihara et al. 2011). This may induce a systematic bias in the estimated radii, surface brightnesses, and concentrations that contaminates the lensing signal. Sky subtraction effects cannot distinguish between foreground and background galaxies (with respect to the bright lens), so this proximity bias can in principle be estimated from the photoFP residuals for galaxies in the foreground of the lenses, which are unaffected by lensing.

Figure 3 shows the average deviation from the photoFP as a function of source-lens angular separation for both foreground and background sources. The sky proximity bias systematically induces a reduction in effective radius relative to the photoFP trend. The lensing signal is thus the difference between the background and foreground photoFP deviations at each angular separation. Of note is the fact that our empirical sky correction extends beyond the size of the SDSS sky subtraction box, which is $\sim 100''$; this is a result of galaxy clustering. Each of the bright objects used as a lens will tend to be associated with a galaxy overdensity on the sky. This excess will also impact the sky correction, even in neighboring sky subtraction cells, so the angular scale of the resulting correction will be set by the galaxy correlation function.

The low redshift of the lens sample and the poor quality of the photo- z 's (which preferentially scatter higher- z sources to lower z) result in a large fraction of source galaxies near lenses with photometric redshifts $z_p < z_l$ that are actually at $z > z_l$. This means that a foreground sample of sources with photo- z 's will be contaminated by objects from higher z . The cut on f_L described above removes many such contaminating galaxies, at the cost of dramatically reducing the signal-to-noise ratio of the sky proximity bias estimate. This remains the major source of uncertainty in this measurement.

As a check against this effect, we also show the deviation from the photoFP trend of those foreground sources with spectroscopic redshifts. Any large bias to this sky subtraction estimate resulting from imperfect photo- z 's should produce a substantial difference between the spectroscopic and photometric foreground estimates; this is

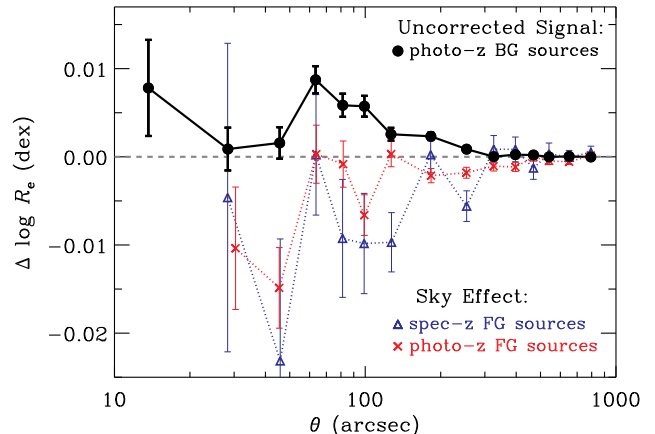


Figure 3. The raw magnification signal around the galaxy lenses (filled black circles) compared with the sky proximity bias measured from foreground sources. The red crosses show the estimated sky subtraction effect using sources with photo- z 's; the blue triangles show the same estimate, but using those foreground galaxies with spectroscopic redshifts.

not observed.

3.4. Halo Mass Profile

After controlling for the systematic errors described above, we calculate the line-of-sight surface matter density Σ by weighting each lens-background source pair by the critical density for lensing, $\Sigma_{\text{crit}}(z_s, z_l)$. We bin this density by physical separation in the lens plane. Our results are shown in figure 4, along with existing measurements from M+06 for a similar lens population.

4. DISCUSSION: THE WAY FORWARD

The magnification signal demonstrated above, while many times stronger than previous magnification measurements, is still somewhat noisier than the shear signal for a comparable sample. This is because the convergence dispersion resulting from the measured photoFP width is 35% (1.8 times larger than the intrinsic shear dispersion of 20%) and because we have only used the third of the source sample consistent with early-type SEDs.

If the fundamental achievable limit for this technique is the intrinsic scatter in the *spectroscopic* fundamental plane, then the average magnification S/N for an early-type galaxy is the same as in shear; a comparable photometric Tully-Fisher relation for late-type galaxies would bring us to the point where magnification and shear provide comparable information. And any improvement in our understanding of galaxy evolution and dynamics that further diminishes the scatter in these scaling relations will boost the magnification signal beyond that available for shear measurement.

Perhaps just as valuable, magnification by this method is not sensitive to the same systematic biases that challenge upcoming shear measurements. For instance, the intrinsic galaxy alignment signal on large scales should not affect galaxy sizes, concentrations, and mean surface brightnesses in the same manner in which it affects shapes. We expect that this technique will also prove useful in extracting and removing instrumental systematics, such as those arising from variations in the telescope point-spread function, and will investigate this prospect in a subsequent paper.

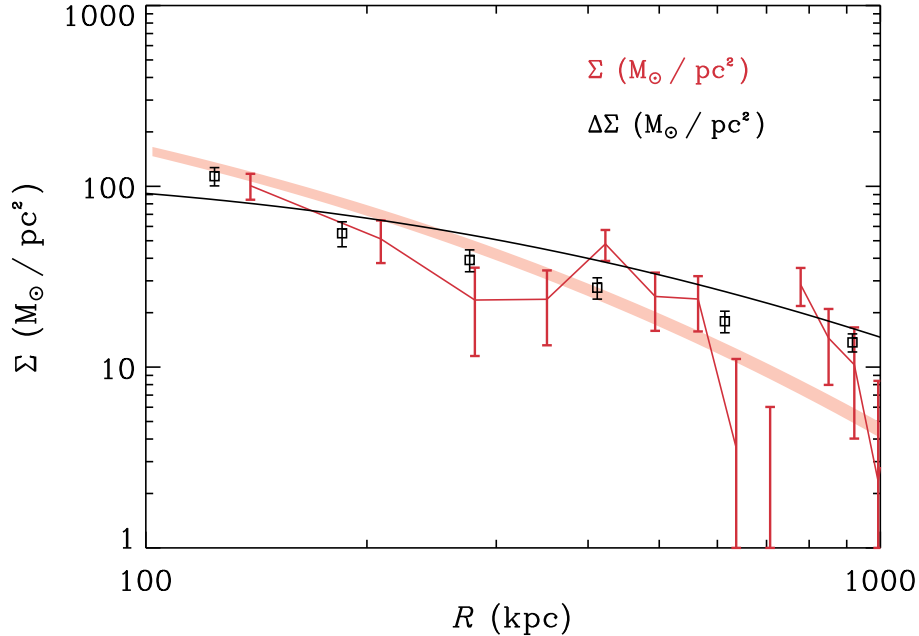


Figure 4. Red points: Σ from this work. Black points: $\Delta\Sigma$ from M+06 measured using shear. That measurement used a smaller lens sample than we consider here, so we have reduced those error bars to allow for a fair comparison with this sample. The solid black line is the best-fit $\Delta\Sigma$ profile from M+06. The shaded red region shows the corresponding Σ profile (with 68% confidence interval) derived from the M+06 data.

The authors are deeply grateful to Rachel Mandelbaum and Reiko Nakajima for their help in understanding several of the systematic errors, and to them and to Chris Hirata for many useful and productive discussions related to this work. The authors are also grateful to the PRIMUS team for allowing the use of their spectroscopic catalog in estimating photometric redshift calibration errors.

E. M. H. is supported by Award #DE-AC02-05CH11231, funded by the Department of Energy's Office of High Energy Physics. G. G. is supported by a fellowship from the Miller Institute for Basic Research in Science.

Funding for SDSS-III has been provided by the Alfred P. Sloan Foundation, the Participating Institutions, the National Science Foundation, and the U.S. Department of Energy. The SDSS-III web site is <http://www.sdss3.org/>.

SDSS-III is managed by the Astrophysical Research Consortium. The Participating Institutions are the American Museum of Natural History, Astrophysical Institute Potsdam, University of Basel, University of Cambridge, Case Western Reserve University, University of Chicago, Drexel University, Fermilab, the Institute for Advanced Study, the Japan Participation Group, Johns Hopkins University, the Joint Institute for Nuclear Astrophysics, the Kavli Institute for Particle Astrophysics and Cosmology, the Korean Scientist Group, the Chinese Academy of Sciences (LAMOST), Los Alamos National Laboratory, the Max-Planck-Institute for Astronomy (MPIA), the Max-Planck-Institute for Astrophysics (MPA), New Mexico State University, Ohio State University, University of Pittsburgh, University of Portsmouth, Princeton University, the United States Naval Observa-

tory, and the University of Washington.

REFERENCES

- Abazajian, K. N., et al. 2009, *ApJS*, 182, 543
- Aihara, H., et al. 2011, *ApJS*, 193, 29
- Bauer, A. H., Seitz, S., Jerke, J., Scalzo, R., Rabinowitz, D., Ellman, N., & Baltay, C. 2011, *ApJ*, 732, 64
- Bell, E. F., McIntosh, D. H., Katz, N., & Weinberg, M. D. 2003, *ApJS*, 149, 289
- Bergé, J., et al. 2008, *MNRAS*, 385, 695
- Bernardi, M., et al. 2003, *AJ*, 125, 1866
- Bertin, G., & Lombardi, M. 2006, *ApJ*, 648, L17
- Blanton, M. R., et al. 2005, *AJ*, 129, 2562
- Bradač, M., et al. 2008, *ApJ*, 681, 187
- Broadhurst, T., Takada, M., Umetsu, K., Kong, X., Arimoto, N., Chiba, M., & Futamase, T. 2005, *ApJ*, 619, L143
- Clowe, D., Bradač, M., Gonzalez, A. H., Markevitch, M., Randall, S. W., Jones, C., & Zaritsky, D. 2006, *ApJ*, 648, L109
- Davis, M., et al. 2003, in Presented at the Society of Photo-Optical Instrumentation Engineers (SPIE) Conference, Vol. 4834, Society of Photo-Optical Instrumentation Engineers (SPIE) Conference Series, ed. P. Guhathakurta, 161–172
- Djorgovski, S., & Davis, M. 1987, *ApJ*, 313, 59
- Dressler, A., Lynden-Bell, D., Burstein, D., Davies, R. L., Faber, S. M., Terlevich, R., & Wegner, G. 1987, *ApJ*, 313, 42
- Eisenstein, D. J., et al. 2003, *ApJ*, 585, 694
- Feldmann, R., et al. 2006, *MNRAS*, 372, 565
- Fischer, P., et al. 2000, *AJ*, 120, 1198
- Fu, L., et al. 2008, *A&A*, 479, 9
- Graham, A. W. 2002, *MNRAS*, 334, 859
- Graves, G. J., & Faber, S. M. 2010, *ApJ*, 717, 803
- Hildebrandt, H., et al. 2011, *ApJ*, 733, 30
- Hoekstra, H. 2007, *MNRAS*, 379, 317
- Hoekstra, H., Yee, H. K. C., & Gladders, M. D. 2004, *ApJ*, 606, 67
- Jain, B., & Lima, M. 2011, *MNRAS*, 411, 2113
- Jee, M. J., et al. 2007, *ApJ*, 661, 728
- Jørgensen, I., Franx, M., & Kjaergaard, P. 1996, *MNRAS*, 280, 167

- Kneib, J., et al. 2003, *ApJ*, 598, 804
Kubo, J. M., et al. 2009, *ApJ*, 702, L110
Le Fèvre, O., et al. 2005, *A&A*, 439, 845
Leauthaud, A., et al. 2010, *ApJ*, 709, 97
Lima, M., Cunha, C. E., Oyaizu, H., Frieman, J., Lin, H., & Sheldon, E. S. 2008, *MNRAS*, 390, 118
Mahdavi, A., Hoekstra, H., Babul, A., Balam, D. D., & Capak, P. L. 2007a, *ApJ*, 668, 806
Mahdavi, A., Hoekstra, H., Babul, A., Sievers, J., Myers, S. T., & Henry, J. P. 2007b, *ApJ*, 664, 162
Mandelbaum, R., Seljak, U., Cool, R. J., Blanton, M., Hirata, C. M., & Brinkmann, J. 2006a, *MNRAS*, 372, 758
Mandelbaum, R., Seljak, U., & Hirata, C. M. 2008a, *JCAP*, 8, 6
Mandelbaum, R., Seljak, U., Kauffmann, G., Hirata, C. M., & Brinkmann, J. 2006b, *MNRAS*, 368, 715
Mandelbaum, R., et al. 2005, *MNRAS*, 361, 1287
—. 2008b, *MNRAS*, 386, 781
Massey, R., et al. 2007, *ApJS*, 172, 239
Ménard, B., Scranton, R., Fukugita, M., & Richards, G. 2010, *MNRAS*, 405, 1025
Okabe, N., & Umetsu, K. 2008, *PASJ*, 60, 345
Parker, L. C., Hoekstra, H., Hudson, M. J., van Waerbeke, L., & Mellier, Y. 2007, *ApJ*, 669, 21
Rozo, E., & Schmidt, F. 2010, *ArXiv e-prints*
Scranton, R., et al. 2005, *ApJ*, 633, 589
Seljak, U., et al. 2005, *Phys. Rev. D*, 71, 043511
Sheldon, E. S., et al. 2004, *AJ*, 127, 2544
—. 2009, *ApJ*, 703, 2217
Shimasaku, K., et al. 2001, *AJ*, 122, 1238
Wake, D. A., et al. 2011, *ApJ*, 728, 46